J. Appl. Comput. Mech., 9(2) (2023) 404-418
DOI: 10.22055/jacm.2022.41157.3709

ISSN: 2383-4536
jacm.scu.ac.ir

Shahid Chamran University of Ahvaz

Journal of Applied and Computational Mechanics

Research Paper

Driveline Stability in Racing Motorcycles: Analysis of a Three Degrees of Freedom Minimal Model

Alexander E. Schramm, Luca Leonelli, Silvio Sorrentino

Department of Engineering Enzo Ferrari, University of Modena and Reggio Emilia, Via Vivarelli 10, Modena, 41125, Italy

Received June 20 2022; Revised September 23 2022; Accepted for publication September 24 2022.
Corresponding author: A.E. Schramm (alexander.schramm@studio.unibo.it)

Abstract. Motorcycles under heavy braking conditions can experience a self-excited oscillation known as 'chatter'. A simplified three degrees of freedom model of the rear of a motorcycle is developed to study the stability of this mode with the inclusion of lateral dynamics introduced by roll angle. Since motorcycles achieve high roll angles during operation, the study of chatter during these manoeuvres is a topic of interest. The equations of motion are linearised about a quasistatic equilibrium and simplified to accommodate symbolic inspection. Power analysis, eigensystem analysis, eigenvalue sensitivity and Routh-Hurwitz stability criterion are used to study the stability of the system in the braking region. It was found that a driveline mode can become unstable at about 19 Hz, and that its tendency towards instability is increased with added roll angle. This mode is sensitive to model parameters affecting the system inertia and stiffness, as well as the chain geometry. Finally, it is found that the lateral dynamics and roll angle play no direct role in chatter but have a significant indirect effect on it through the working point of the force characteristic function of the tyre.

Keywords: Motorcycle dynamics; stability; chatter; driveline; roll angle.

1. Introduction

Motorcycles and single-track vehicles are complex systems that can present difficult stability problems, the modelling and prediction of which is a subject of great interest [1]. Specifically in high performance and racing motorcycles, there exists lightly damped or unstable oscillatory motions of front and rear wheels experienced during heavy braking manoeuvres which are typically denoted 'patter' and 'chatter,' respectively. For chatter, though mitigation of the phenomenon might be achieved through improved damper technology [2], it is also important to understand the causes and mechanisms of the instability, including possible sources from both in-plane and out-of-plane dynamics. This unstable mode typically has a frequency of 17 Hz to 22 Hz. Tezuka et al. [3] used a full multibody model to characterise the instability as out of phase oscillations of the sprung mass on the suspension springs and the unsprung masses on the vertical stiffness of the tyres, during running manoeuvres. Later, Catania and Mancinelli [4, 5] produced an in-plane multibody model that was used to numerically time-integrate a heavy braking manoeuvre. In [4], root loci were used to show the interaction of tyre parameters with the damping of the rear hop mode, as well as the coupling of the front and rear modes, and the effect on stability of the swingarm length was also investigated. In [5], the model was numerically integrated, and the instability was shown to rise from interaction between tyre forces and torsional vibrations of the tyre.

Cossalter et al. [6, 7] were the first to introduce a viscoelastic transmission element and showed via both root loci and numerical simulation that this created an additional driveline mode that shared similar frequency and lighter damping than the rear hop mode. In contrast, Sharp and Watanabe [8] used a commercial multibody software to show that an instability of around 25 Hz occurs with sufficient torsional compliance in the steering head, affecting mainly the front wheel during high lateral acceleration operation. Catania et al. [9] expanded their previous model into a full out-of-plane multibody model using numerical integration and linearised root loci to study the stability of the chatter mode. It was concluded that a vertical load dependent longitudinal relaxation length can cause a phase lag between vertical and longitudinal forces, able to destabilize the system.

Leonelli [10] introduced a simplified planar model to study the phenomenon analytically. This model, including rear wheel spin, vertical rear suspension travel and a chain drive component, was used to examine the stability regions analytically. It was found that the phase relationship between tyre forces brought upon by a variable relaxation length and chain forces are the cause of chatter instability. For comparison, a full multibody simulation was also presented, similar to that of [9]. Further, in [11], the authors examine three models of increasing complexity and conclude that the tyre longitudinal slip gradient can be a cause of instability even with constant relaxation length. In [12], the authors return to the two degrees of freedom model presented in [10], but add in a more complete chain drive geometry, as well as considering a null relaxation length. Within, the stability boundaries are studied analytically, and it was determined that instability exists despite the lack of relaxation length and is caused by the phase lag introduced by asymmetric stiffness matrices in the linearised equations of motion. This is driven by the tyre vertical and longitudinal slip force gradients. In [13] these findings were validated using a planar multibody model. Again, no relaxation length

Published online: October 04 2022

was considered, and the relevant stability boundaries and important parameters were compared to the two degrees of freedom model, showing close relation. The similar patter phenomenon at the front wheel was investigated by the authors in [14].

The objective of this study is to investigate the roles, if any, that motorcycle roll angle and tyre lateral force dynamics play in the stability of the chatter mode. Motorcycles, specifically racing machines, tend to experience large non-negligible roll angles [15], and therefore it is of practical interest to understand whether or not a static roll angle, or in fact a roll angle degree of freedom, is required to fully predict the behaviour of this mode. This study will extend the two degrees of freedom model presented in [12] to three degrees of freedom with the addition of a roll angle, with the study of driveline stability at increasing roll angles and the possible interactions of the lateral dynamics being the topics of interest. This study seeks to show the effects of both a varying static lean angle and the role lateral force oscillations play on the stability of the chatter mode. To this purpose, an adequate tyre model has been adopted, according to Pacejka [16] (Magic Formula). To date, the studies investigating the driveline mode have done so only in straight braking manoeuvres. It is anticipated that the addition of roll angle will also allow the minimal model to predict instabilities of the rear system in more than just braking manoeuvres, such as in cornering and acceleration manoeuvres, topics for future studies. This paper will present the full equations of the new model in section 2 and demonstrate its use analysing a braking manoeuvre. Section 3 compares the minimal model to a full multibody simulation and provides the resulting stability analysis of the minimal system, as well as some root cause investigations and parameter sensitivities.

2. Model Description

The model in this study is developed as an extension to that of Sorrentino and Leonelli [12]. The roll angle of a motorcycle in a curve is added as a third degree of freedom in the model, accompanied by some nomenclature and methodology changes due to the increased complexity.

The geometry of the model is presented in Fig. 1, which show rear and planar (aligned with roll angle ϕ) views. The model represents the rear part of a motorcycle, which in this case is attached to an infinite inertia frame, translating, and rotating with stationary velocities V_{fx}, V_{fy}, and Ω_{fz} on a perfectly flat plane. In the model, stationary values for velocities are imposed even though a braking torque on the rear wheel is present, in order to get the stationary operating points necessary for performing stability analysis. The reference frame is attached to the infinite inertia frame and given in x-forward, y-right, z-down SAE convention. On this frame at point F, at a height of z_f from the ground plane, is a revolute joint aligned parallel with x-axis. To this joint connects the first part of the rear frame which serves to model the main mass of the motorcycle, onto which is attached the front sprocket of the drivetrain, whose radius is r_p. This member is defined by the joint's angle ϕ and the line FS, whose geometry is defined by x_f and h_f. The mass of the reference frame m_{fr} is located a fraction η_{fr} down its length from point F, and the reference system in which its inertia matrix $\mathbf{J}_{fr}$ is defined is aligned along the x-axis with its z-axis rotated through ϕ to remain in-plane with the rest of the system. At point S there is a revolute joint perpendicular to the x-axis and the line FS, this is the swingarm pivot. The swingarm is represented by the line SA, with a length of l_{sa} and an angle α of the joint. The swingarm's mass m_{sa} is located a fraction η_{sa} along line SA, and the reference system in which the inertia matrix $\mathbf{J}_{sa}$ is aligned has its x-axis along the line SA while its z-axis remains in-plane with the system. Connected at point A is the final revolute joint which is parallel to swingarm pivot. This joint connects the body representing the wheel, tyre, and rear sprocket. This body is characterised by the joint's angle θ (which breaks convention and is aligned along the negative y-axis, so that wheel rotation is positive with motion in the forward x-direction), the outer radius of the tyre R_r, the toroid radius of the tyre ρ_r, and the rear sprocket radius r_c. The rear wheel mass m_{wh} is centred at point A, and the reference system in which the inertia matrix $\mathbf{J}_{wh}$ is aligned has its y-axis aligned with the revolute joint and is symmetric about that axis. All inertia matrices $\mathbf{J}_i$ are assumed to be in the principal axes, with no cross-terms.

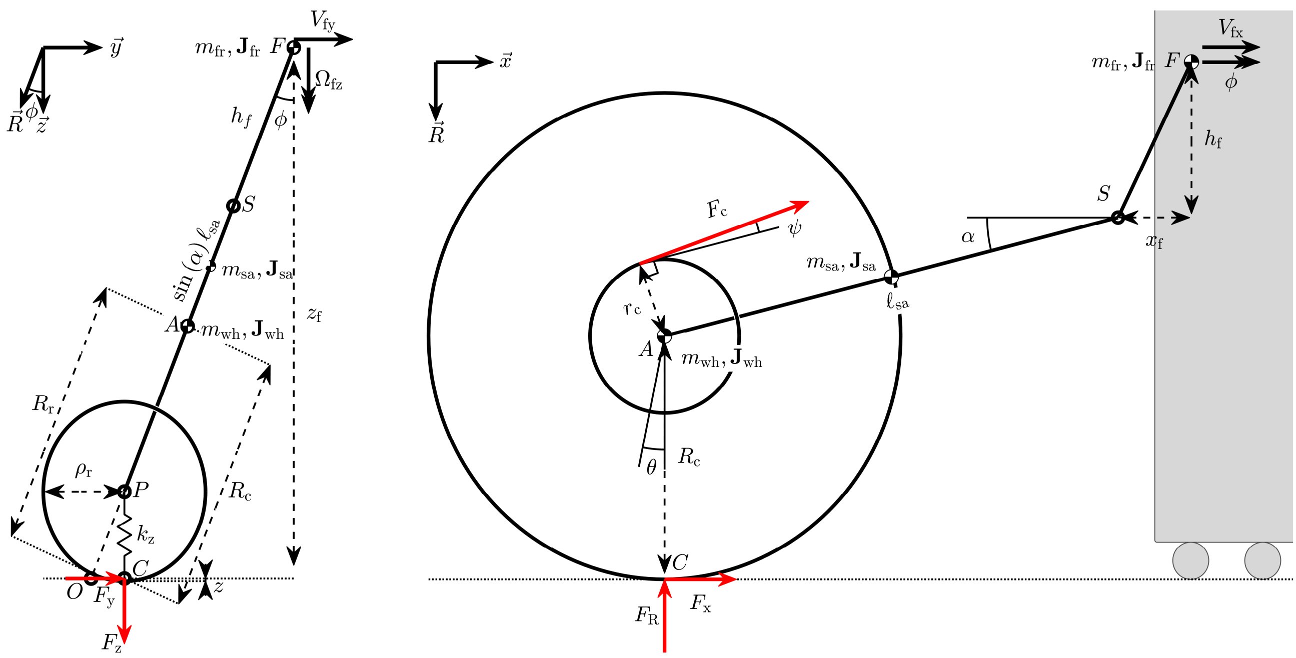

(a) Rear view (b) Planar side view

Fig. 1. Model free body diagrams shown in acceleration condition.

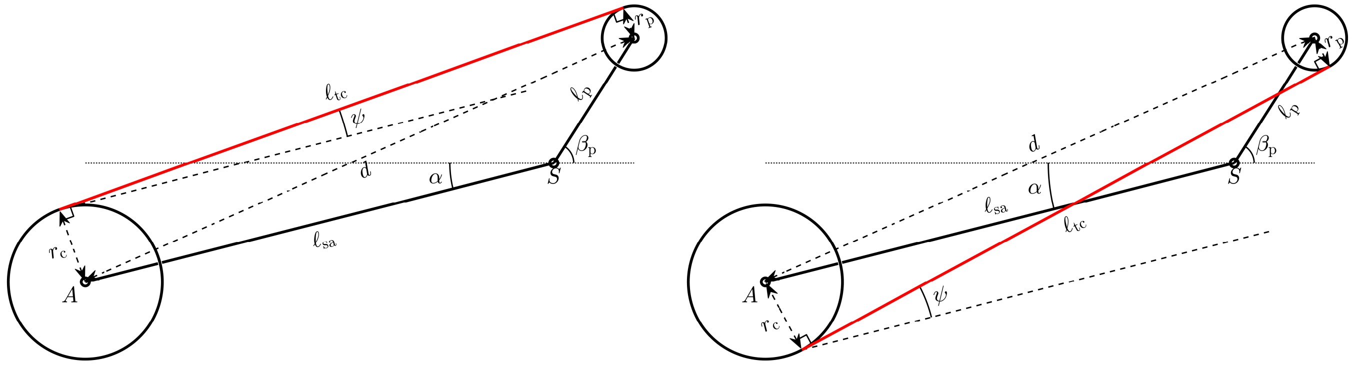

(a) $\delta = -1$ (acceleration) (b) $\delta = 1$ (braking)

Fig. 2. Geometry of the drivetrain.

The kinetics of the model are given corresponding to the three degrees of freedom: α, θ and ϕ. The non-constraint forces and moments in this model consist of the tyre forces (F_x, F_y, and F_z), chain force (F_c), braking moment (M_{brake}), swingarm rotational spring and damper acting on joint S (k_s and c_s), and the optional frame rotational spring and damper acting on joint F (k_f and c_f). The equations of motion are formulated using the Lagrange equations as outlined in [17, 18], and are given by:

$$\begin{aligned} J_\alpha \ddot{\alpha} &= l_{sa}\cos(\alpha)\cos(\phi)(m_{wh} + \eta_{sa} m_{sa})g + M_{cent,\alpha} + M_{cor,\alpha} + M_{gyro,\alpha} \\ &\quad - l_{sa}\sin(\psi(\alpha))k_c(l_c(\alpha,\theta) - l_{fc}) + l_{sa}\sin(\alpha)F_x(\mathbf{q},\dot{\mathbf{q}}) - l_{sa}\cos(\alpha)F_R(\mathbf{q},\dot{\mathbf{q}}) - k_s(\alpha - \alpha_{s0}) - c_s\dot{\alpha} - M_{brake} \end{aligned} \tag{1}$$

$$J_{why}\ddot{\theta} = -J_{why}\cos(\phi)\Omega_{fz}\dot{\phi} - \delta r_c k_c(l_c(\alpha,\theta) - l_{fc}) - R_c(\alpha,\phi)F_x(\mathbf{q},\dot{\mathbf{q}}) - M_{brake} \tag{2}$$

$$\begin{aligned} J_\phi \ddot{\phi} &= -\sin(\phi)[h_f(m_{wh} + m_{sa} + \eta_{fr} m_{fr}) + l_{sa}\sin(\alpha)(m_{wh} + \eta_{sa} m_{sa})]g + M_{cent,f} + M_{cor,f} + M_{gyro,f} \\ &\quad - z_f F_y(\mathbf{q},\dot{\mathbf{q}}) - (h_f + l_{sa}\sin(\alpha) + R_r - \rho_r)\sin(\phi)F_z(\mathbf{q},\dot{\mathbf{q}}) - k_f(\phi - \phi_{f0}) - c_f\dot{\phi} \end{aligned} \tag{3}$$

where $\mathbf{q}$ represents the vector of degrees of freedom, (α, θ, ϕ) , g is acceleration due to gravity, l_{fc} and l_c represents the free and dynamic total length of the chain respectively, while the variable δ determines the active portion of the chain (1 for braking and −1 for acceleration), α_{s0} and ϕ_{f0} give the spring preloads, J_α and J_ϕ are reduced inertia and the inertia elements ($M_{cent,i}$, $M_{cor,i}$, $M_{gyro,i}$) are collected here but are negligible and omitted hereafter due to their numerical insignificance. Finally, F_R and R_c can be solved for geometrically:

$$F_R(\mathbf{q},\dot{\mathbf{q}}) = \sin(\phi)F_y(\mathbf{q},\dot{\mathbf{q}}) - \cos(\phi)F_z(\mathbf{q},\dot{\mathbf{q}}) \tag{4}$$

$$R_c(\alpha,\phi) = R_r - \rho_r + \cos(\phi)(\rho_r - z(\alpha,\phi)) \tag{5}$$

$$z(\alpha,\phi) = \cos(\phi)(h_f + l_{sa}\sin(\alpha) + R_r - \rho_r) - z_f + \rho_r \tag{6}$$

while the other dependent terms need further derivation, as shown in the subsequent sections.

2.1 Chain Geometry

The chain is modelled as a spring wrapped around two wheels (the front and rear sprockets) with no slip. Chain damping is neglected, as the term tends to be small in chain systems [19]. The length of the spring l_c varies as the wheels spin, and as the configuration geometry changes due to variations in the generalized coordinates. Typical chain geometries are shown in Fig. 2, both in the acceleration and braking cases. Shown is the swingarm with length l_{sa} and angle α, at the end of which is the rear sprocket with a radius of r_c. The front sprocket is held offset from the swingarm pivot by a distance of l_p and an angle of β_p from the horizontal and has a radius of r_p. Also shown in the figure is the centre distance between the sprockets d, the chain tangential distance l_{tc}, and the chain angle ψ while in acceleration ($\delta = -1$). The equations for chain geometry are given by:

$$l_c(\alpha,\theta) = l_{tc}(\alpha) - \delta(r_p - r_c)(\alpha + \psi(\alpha) + \psi(0)) - \delta(r_p\theta_p - r_c\theta) \tag{7}$$

$$\sin(\psi(\alpha)) = \frac{l_{tc}(\alpha)l_p\sin(\beta_p - \alpha) - \delta(r_p - r_c)(l_{sa} + l_p\cos(\beta_p - \alpha))}{d(\alpha)^2} \tag{8}$$

$$l_{tc}(\alpha)^2 = d(\alpha)^2 - (r_p - r_c)^2 \tag{9}$$

$$d(\alpha)^2 = l_{sa}^2 + l_p^2 + 2l_{sa}l_p\cos(\beta_p - \alpha) \tag{10}$$

2.2 Tyre Model

The tyre is modelled geometrically as a torus with minor radius ρ_r and major radius ($R_r - \rho_r$). Tangential (F_x, F_y) and normal (F_z) forces are produced at the tyre contact point C. In this study the tyre moments (overturning, self-aligning, and rolling resistance) are neglected. Lateral and longitudinal deflections of the tyre carcass and contact point are also neglected. Relaxation length is considered small enough in racing tyres as to be neglected, as demonstrated by [11]. Rigid ring tyre models are not used as they have been demonstrated as unnecessary for the modes of interest [20].

Normal force is produced by vertical deflection in the tyre carcass in the z-direction, similar to the MF-MCTire model presented by Schmeitz et al. [21]:

$$F_z(\mathbf{q},\dot{\mathbf{q}}) = -k_z z(\alpha,\phi) \tag{11}$$

In this study, theoretical tyre slips will be used (σ_x, σ_y, φ as used in chapter two of [22]) due to the ease of use when deriving equations. Further, tyre camber reduction factor ε_r is assumed to be zero and spin slip (φ) is assumed to have negligible effect on the forces. Tyre tangential forces are produced based on the system kinematics given by generalised functions $F_x(\sigma_x, \sigma_y, F_z, \phi)$ and $F_y(\sigma_x, \sigma_y, F_z, \phi)$, which are chosen to be the magic formulae given by Pacejka [16]. The full nonlinear forms of these equations are used in the calculation of equilibrium conditions, but for the linearised model only the Taylor expansion terms are required and are presented here for clarity.

Given the tyre force gradients $C_{\sigma_x,x}$, $C_{\sigma_y,x}$, $C_{F_z,x}$, $C_{\phi,x}$, $C_{\sigma_x,y}$, $C_{F_z,y}$, and $C_{\phi,y}$, and introducing the congruence equations and their derivatives, the required tyre force variation equations are:

$$\tilde{F}_x(\dot{\tilde{\alpha}},\dot{\tilde{\phi}},\dot{\tilde{\theta}},\tilde{\alpha},\tilde{\phi}) = \left[\frac{l_{sa}\cos(\alpha_0)}{R_{R0}\omega_0}(\tan(\alpha_0)C_{\sigma_x,x} - \sin(\phi_0)C_{\sigma_y,x})\right]\dot{\tilde{\alpha}} - \frac{\chi_x}{\omega_0}\dot{\tilde{\theta}} - \frac{z_f}{R_{R0}\omega_0}C_{\sigma_y,x}\dot{\tilde{\phi}} - l_{sa}\cos(\alpha_0)k\lambda_{x1}\tilde{\alpha} + (L_R\cos(\phi_0)k\lambda_{x2})\tilde{\phi} \tag{12}$$

$$\tilde{F}_y(\dot{\tilde{\alpha}},\dot{\tilde{\phi}},\dot{\tilde{\theta}},\tilde{\alpha},\tilde{\phi}) = \left[\frac{l_{sa}\cos(\alpha_0)}{R_{R0}\omega_0}(\tan(\alpha_0)C_{\sigma_x,y} - \sin(\phi_0)C_{\sigma_y,y})\right]\dot{\tilde{\alpha}} - \frac{\chi_y}{\omega_0}\dot{\tilde{\theta}} - \frac{z_f}{R_{R0}\omega_0}C_{\sigma_y,y}\dot{\tilde{\phi}} - l_{sa}\cos(\alpha_0)k\lambda_{y1}\tilde{\alpha} + (L_R\cos(\phi_0)k\lambda_{y2})\tilde{\phi} \tag{13}$$

where the subscript 0 defines a stationary operating point while the diacritic ~ is used to define the perturbation portion of the Taylor expansion, ω is the wheel speed, R_R the rolling radius, χ_i and λ_{ij} are compact notation of the tyre gradient terms (defined in the appendix), k is a 'total system stiffness' (defined in the appendix), and L_R is given as:

$$L_R = h_f + l_{sa}\sin(\alpha_0) + R_r - \rho_r \tag{14}$$

2.3 Model Linearisation

To assess the stability of the minimal model, the eigenvalues of the linearised system are used. The system is assumed to contain only small oscillations about a stationary operating point and therefore a Taylor series approximation is applied. Taking the Jacobian of Eqns. (1)-(3) and substituting for the formulae found in Eqns. (4)-(14) gives the linearised equations of motion about an operating point, actually an equilibrium point (denoted by the subscript 0). To simplify the expressions, the rotational coordinates are transformed into linear displacements using characteristic lengths. The equations of motion are expressed with non-dimensional parameters normalized to the swingarm degree of freedom. This eases the ensuing calculations and their readability. The new coordinates and their characteristic lengths are given by:

$$\mathbf{q} = \begin{Bmatrix} l_\alpha\tilde{\alpha} \\ R_{R0}\tilde{\theta} \\ l_f\tilde{\phi} \end{Bmatrix}, \quad \begin{cases} l_\alpha = l_{sa}\cos(\alpha_0) \\ l_f = L_R\cos(\phi_0) \end{cases} \tag{15}$$

Trigonometric expressions are shortened to c_x, s_x and τ_x for cos(x), sin(x), and tan(x), respectively. The simplified equations of motion are given as:

$$\mathbf{M}\ddot{\mathbf{q}} + (\mathbf{C} + \mathbf{C}_{\text{tyre}})2\zeta\omega_n\dot{\mathbf{q}} + (\mathbf{K} + \mathbf{K}_{\text{chain}} + \mathbf{K}_{\text{tyre}})\omega_n^2\mathbf{q} = \mathbf{0} \tag{16}$$

where ω_n is a resulting natural frequency of the normalisation, ζ the damping ratio, and the matrices are given by:

$$\begin{gathered}
\mathbf{M} = \begin{bmatrix} 1 & 0 & 0 \\ 0 & I_\theta & 0 \\ 0 & 0 & I_\phi \end{bmatrix}, \quad \mathbf{C} = \begin{bmatrix} 1 & 0 & 0 \\ 0 & 0 & 0 \\ 0 & 0 & \psi_f \end{bmatrix}, \quad \mathbf{C}_{\text{tyre}} = \begin{bmatrix} -\tau_\alpha^2\gamma_{xx} + \tau_\alpha s_\phi(\gamma_{xy} + \gamma_{yx}) - s_\phi^2\gamma_{yy} & \tau_\alpha\Gamma_x - s_\phi\Gamma_y & \xi_z(\tau_\alpha\gamma_{xy} - s_\phi\gamma_{yy}) \\ \tau_\alpha\gamma_{xx} - s_\phi\gamma_{xy} & -\Gamma_x & -\xi_z\gamma_{xy} \\ \xi_z(\tau_\alpha\gamma_{yx} - s_\phi\gamma_{yy}) & -\xi_z\Gamma_y & -\xi_z^2\gamma_{yy} \end{bmatrix} \\
\mathbf{K} = \begin{bmatrix} 1 & 0 & -s_\phi(\Phi_z - g_{\alpha\phi}) \\ 0 & 0 & 0 \\ -s_\phi(\Phi_z - g_{\alpha\phi}) & 0 & \Phi_f + \tau_\phi^2\Phi_z + g_\phi \end{bmatrix}, \quad \mathbf{K}_{\text{chain}} = \Phi_c\begin{bmatrix} \xi_R\sigma^2(1+\sigma') & \delta\sigma & 0 \\ \delta\xi_R\sigma & 1 & 0 \\ 0 & 0 & 0 \end{bmatrix}, \quad \mathbf{K}_{\text{tyre}} = \begin{bmatrix} \tau_\alpha\lambda_{x1} - s_\phi\lambda_{y1} & 0 & -(\tau_\alpha\lambda_{x2} - s_\phi\lambda_{y2}) \\ -\lambda_{x1} & 0 & \lambda_{x2} \\ -\xi_z\lambda_{y1} & 0 & \xi_z\lambda_{y2} \end{bmatrix}
\end{gathered} \tag{17}$$

where the simplified compact notation terms are the normalised inertiae I_i, a normalised frame rotational damping ψ_f, near-unity geometric factors ξ_i, tyre force gradient damping terms γ_{ij} and Γ_i, normalized stiffnesses Φ_i, gravitational terms g_{ij}, chain geometry terms σ and σ', and tyre force gradient terms λ_{ij}. Note that there is an additional tyre force stiffness matrix arising from the stationary tyre forces, but it is omitted here due to its numerical insignificance.

The role of the linearised tyre forces Eqns. (12) and (13) are shown in the $\mathbf{C}_{\text{tyre}}$ and $\mathbf{K}_{\text{tyre}}$ matrices. Effective damping terms from the tyre forces arise from the tyre gradients, given by γ_{ij}, which are the reduced gradients of tyre force i in slip j ($C_{\sigma j,i}$), and Γ_i which are linear combinations of the γ_{ij} based on operating conditions. Similarly, force gradient terms from the tyre arise from λ_{ij}, which depend on the tyre tangential force gradient due to vertical load ($C_{Fz,i}$). The stiffness matrix $\mathbf{K}_{\text{chain}}$ represents the terms due to chain stiffness (Φ_c) and chain geometry (σ, which depends on the chain-to-swingarm angle ψ). The definitions of the compact notation terms are reported in the appendix.

2.4 Stationary Conditions

In order to study the stability of the linearized model, it is required to extract quasistatic conditions from a time-varying manoeuvre performed by a motorcycle in simulation. According to Rosenbrock [23], in time-varying systems the real part of the eigenvalues is no longer a sufficient condition for stability and an additional bound exists on the size of the time derivative of the system matrix. In vehicle braking conditions, Salisbury [24] has shown this additional bound causes a slight change in the stability boundary from that found using frozen-time eigenvalue analysis. To reduce the likelihood of any discrepancy in stability boundaries, the quasistatic conditions are selected to be where the operating conditions are slowly varying, namely the tyre tangential forces. While this limitation means the definitive stability of the system requires an extra condition, the eigenvalue method remains a sufficient predictor for system *instability*. For this study, the stationary conditions are obtained from an optimal manoeuvre as calculated by the model developed by Leonelli and Limebeer [25]. A simple 180° corner trajectory is obtained from an optimal control problem, considering the limitations of rider, motorcycle model, and track. The result is shown in Fig. 3. The selected braking region is highlighted in red and occurs during the front rollover limit where tyre forces remain nearly constant. This area of operation has been experimentally shown to exhibit the instability in question, when tyre vertical load is near its minimum and a small longitudinal braking force is applied to the wheel through the chain [13].

This optimal data set gives the required tyre forces, slips, and parameters as well as the kinematics of the frame. The tyre force gradient parameters are given in the practical slip convention and need to be converted using:

$$\begin{aligned} C_{\sigma_x,x} &= -(\kappa+1)^2 C_{\kappa,x}, \quad C_{\sigma_y,x} = -\cos^2(\alpha_{slip})(\kappa+1)C_{\alpha_{slip},x} \\ C_{\sigma_x,y} &= -(\kappa+1)^2 C_{\kappa,y}, \quad C_{\sigma_y,y} = -\cos^2(\alpha_{slip})(\kappa+1)C_{\alpha_{slip},y} \end{aligned} \tag{18}$$

The nonlinear equations of motion (1)-(3) are used for the remaining equilibrium values. α_0 is found geometrically using Eqn. (6) with z given by Eqn. (11) (F_{z0} is provided by the optimal data set):

$$\sin(\alpha_0) = \frac{1}{l_{sa}}\left(\frac{-F_{z0}k_z^{-1} - \rho_r + z_f}{\cos(\phi_0)} - h_f - R_r + \rho_r\right) \tag{19}$$

The equilibrium chain stretch Δl_c is found with Eqn. (2), balancing the tyre force. The optimal manoeuvre data does not include the braking moment M_{brake} and its effects on tyre loads, so it is set to zero. The equilibrium chain stretch is then given as:

$$\Delta l_c = \frac{R_{c0}}{k_c r_c}|F_{x0}| \tag{20}$$

With these data the model has all that is required to solve for quasistatic equilibrium states.

3. Results and Discussion

3.1 Comparison to a multibody Model

To validate the addition of the roll angle to the minimal model, data is extracted from a full multibody simulation as provided by the commercial software VI-Motorcycle and used to compare to the results of the minimal model. The multibody simulation consists of a full rigid-body model of a motorcycle as provided by VI, includes 37 degrees of freedom, and is operated in a braking manoeuvre similar to (but not exactly the same as) that provided in section 2.4. The frozen-time eigenvalues at multiple points are extracted and compared to those the minimal model produces using the same input data and model parameters. The results are compared in Fig. 4.

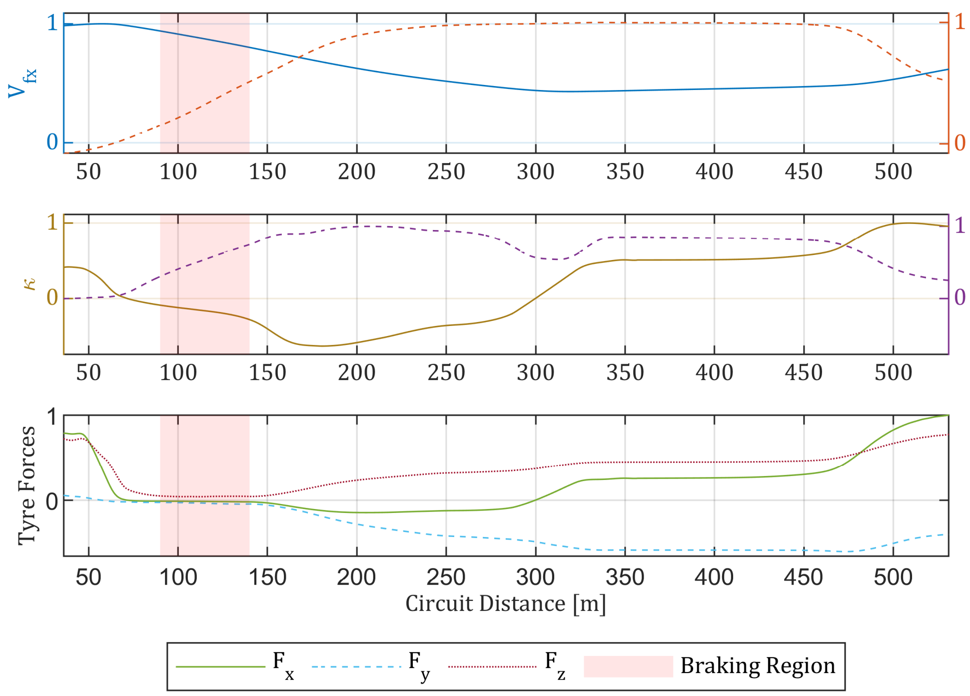

Fig. 3. Manoeuvre used to extract quasistatic equilibrium states, as computed by Leonelli and Limebeer [25]. Y-axes have been normalised due to confidentiality agreements. The braking region used is highlighted in red.

It can be seen that mode one of the minimal model is a pseudo-mode that captures the lower frequency modes of the multibody model, such as bounce and pitch , while mode two and mode three show similar values and behaviour to the rear hop and driveline modes, respectively. The driveline mode from the minimal model does show less stability and a lower frequency than that of the multibody simulation. This is attributed to two things: first, the multibody simulation uses a small chain damping term, moving the eigenvalues slightly towards stability. This is assumed to be a negligible addition which only acts to add a small amount of stability to the system, while not affecting the overall behaviour. Second, the multibody simulation also includes powertrain rotational dynamics, whereas the minimal model assumes an infinite inertia drivetrain. This results in a lower perceived driveline frequency in the minimal model. The most effective way of accommodating for this discrepancy is to raise the chain stiffness or lower the wheel inertia of the minimal model accordingly. These adjustments have shown to accurately represent the modal frequency of the driveline oscillations of the multibody model, without affecting the behaviour of the other modes.

3.2 Minimal Model Analysis

This section will focus on the analysis of the linearised model during the exact quasistatic manoeuvre provided in section 2.4, using parameters from that dataset. The eigenvalue analysis of the quasistatic braking region is presented in Fig. 5. The first mode is similar to that of "Bounce" and has been denoted such. The second mode is a rear hop mode with frequencies of 14 Hz to 17 Hz, and the third mode is the driveline mode with frequencies in the neighbourhood of 19 Hz that begins stable then crosses the stability boundary. This region of the manoeuvre progresses through a forward speed of 260 km/h to 220 km/h, a static roll angle of 8° to 26°, a swingarm angle of 14.3° to 10.6°, and has an average normal load on the tyre of 134 N. Figure 5 also contains the eigenvectors and their evolution through the manoeuvre in the form of polar plots. The bounce mode (Fig. 5b) mainly contains the roll angle oscillations, with an increased presence of swingarm angle as the manoeuvre progresses. The rear hop mode (Fig. 5c) is driven primarily by swingarm oscillations, though as the manoeuvre progresses and static roll angle increases, there is a larger presence of both wheelspeed and roll angle oscillations, suggesting interactions between the modes. Finally, the driveline mode (Fig. 5d) has its main contribution come from the wheelspeed oscillations, the major factor in determining the chain and tyre forces, while also having a small contribution from the swingarm oscillations. In the sequel, focus is put on the stability of the driveline mode, which represents the chattering experienced during heavy braking.

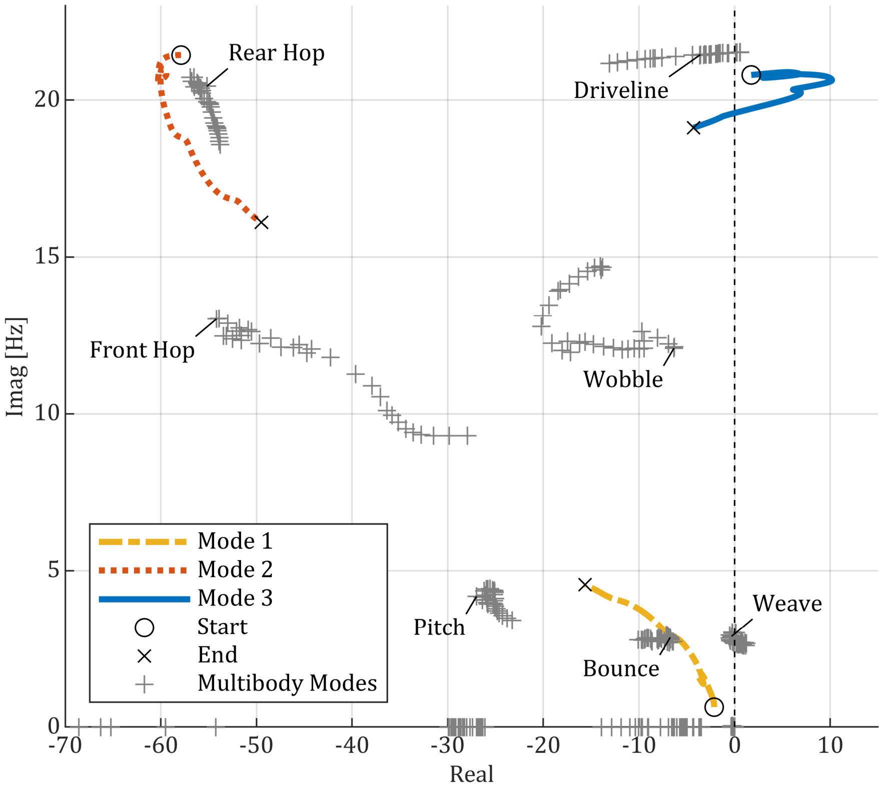

Fig. 4. Comparison of the minimal model eigenvalues with those of a multibody simulation.

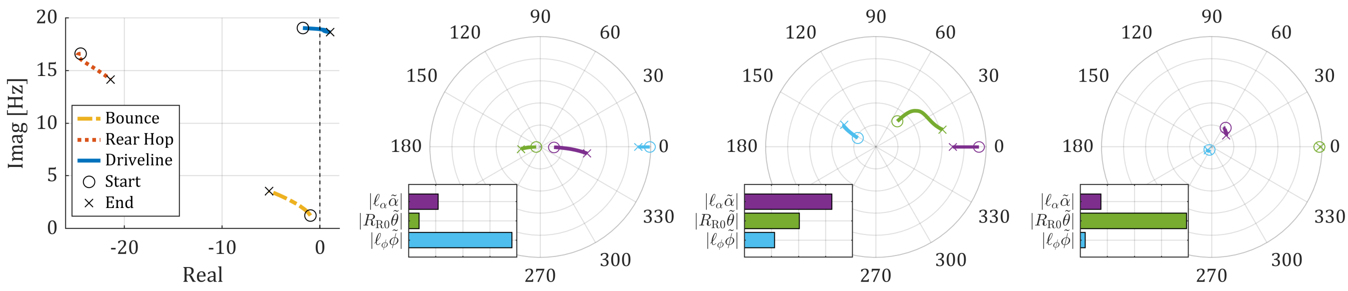

(a) Eigenvalues (b) Bounce eigenvector (c) Rear hop eigenvector (d) Driveline eigenvector

Fig. 5. Quasistatic linear model eigenvalue analysis of the braking region. Evolution of the eigenvectors are shown normalized and phased to their largest component, while the bar chart legends show the average component magnitudes.

3.3 Energy Analysis

To investigate the source of instability, an energy balance method is employed, as in [12] and [26]. If there exists a switching mechanism whose energy flow into the system is greater than that dissipated over one oscillation cycle, vibration amplitude increases. First, recall the linearized equations of motion (16) and recast them with the tyre force terms separated:

$$\mathbf{G} = \mathbf{M}\ddot{\mathbf{q}} + \mathbf{C}\dot{\mathbf{q}} + \left(\mathbf{K} + \mathbf{K}_{\text{chain}}\right)\mathbf{q} - \left(\mathbf{f}_{\text{x}} + \mathbf{f}_{\text{y}}\right) = \mathbf{0} \tag{21}$$

where $\mathbf{q}$ is the vector of system coordinates, $\mathbf{M}$ the mass matrix, $\mathbf{C}$ the damping matrix due to dissipative elements (in this case the damper), $\mathbf{K}$ and $\mathbf{K}_{chain}$ the matrices of conservative elastic elements (springs), while $\mathbf{f}_x$ and $\mathbf{f}_y$ are vectors arising from the tyre tangential ground forces in the longitudinal and lateral directions, respectively. Note that $\mathbf{f}_x$ and $\mathbf{f}_y$ are linearised vectors containing state-dependent non-stationary components, and therefore are not considered as external forces, but as dissipative elements in the linearised equations.

At the stability boundary, the free response of the system converges to harmonic oscillation with a period of *T*. The energy balance over one period can be expressed as:

$$\Delta E = \Delta E_{\text{kin}} + \Delta E_{\text{pot}} + \Delta E_{\text{dis}} = \int_0^{\text{T}} \mathbf{G}\dot{\mathbf{q}}\,dt = 0 \tag{22}$$

where ΔE_{kin} and ΔE_{pot} are the change in kinetic and potential energies over one cycle. If the corresponding matrices are symmetric, then these terms will be zero. For this analysis, the asymmetry of the chain matrix is assumed to be negligible $(\xi_{\text{R}} = 1)$. It follows that:

$$\Delta E_{\text{dis}} = \int_0^{\text{T}} \left[\dot{\mathbf{q}}^{\text{T}}\mathbf{C}\dot{\mathbf{q}} - \dot{\mathbf{q}}^{\text{T}}(\mathbf{f}_{\text{x}} + \mathbf{f}_{\text{y}})\right] dt = 0 \tag{23}$$

which means that over one period of oscillation, the energy dissipated by the damper is balanced by the energy introduced by the ground force terms. If we cast $\mathbf{f}_x$ and $\mathbf{f}_y$ as $\mathbf{a}\tilde{F}_{\text{x}}$ and $\mathbf{b}\tilde{F}_{\text{y}}$, where $\tilde{F}_{\text{i}}$ are the oscillating portion of the ground forces, and $\boldsymbol{a}$ and $\boldsymbol{b}$ are transformation vectors arising from the equations of motion, Eqn. (23) can be reformed as:

$$\int_0^{\text{T}} \left[\dot{\mathbf{q}}^{\text{T}}\mathbf{C}\dot{\mathbf{q}} - \tilde{V}_{\text{sx}}\tilde{F}_{\text{x}} + \tilde{V}_{\text{sy}}\tilde{F}_{\text{y}})\right] dt = 0, \quad \begin{cases} \tilde{V}_{\text{sx}} = \mathbf{a}\cdot\dot{\mathbf{q}} \\ \tilde{V}_{\text{sy}} = \mathbf{b}\cdot\dot{\mathbf{q}} \end{cases} \tag{24}$$

where the oscillating slip velocities $\tilde{V}_{\text{sx}}$ and $\tilde{V}_{\text{sy}}$ have been introduced as a result. Due to the harmonic motion, the latter two terms in the first of Eqn. (24) will be products of two cosine waves of equal frequencies and distinct phase offsets. It can be shown that for the multiplication of cosine waves with relative offset, the result contains a constant term proportional to the cosine of that offset. This allows for a non-zero result of the integration and therefore can cause positive energy flow into the system during phase offsets between -90° and 90°, and energy dissipation outside of this range. Therefore, the source of an instability must come from the phase offset between tyre tangential forces and tyre slips, as described more generally in [26]. Even though the tyre is a dissipative element (as a friction element), under the combined effect of oscillating ground and vertical forces acting with certain values of phase-lag, it can become the channel of an energy flow feeding the system and sustaining a self-excited oscillation. In general, this kind of switching mechanism to instability is classified as 'due to normal fluctuating forces', as explained in [26]. In the specific case of the present analysis, the external source of energy able to sustain the self-excited oscillation is the kinetic energy of the frame, travelling at imposed constant speed.

The tyre force and slips for both tangential directions at the stability boundary are given in Fig. 6a and Fig. 6b. Phase offset in the *x*-direction is found to be approximately 53.6° resulting in energy flow into the system. The phase offset in the *y*-direction is 90.8° resulting in an insignificant energy dissipation.

The source of the offset in the *x*-direction is the phase that exists between the tyre normal load $\tilde{F}_{\text{z}}$ and the longitudinal slip velocity $\tilde{V}_{\text{sx}}$, and the fact that the longitudinal force is made up of a weighted linear combination of these terms (through the coefficients $C_{\sigma_x,x}$ and $C_{F_z,x}$). The phase relationship between normal load and tyre slip is displayed in Fig. 6c to Fig. 6f. There it is shown that slip is largely dependent on the $\dot{\tilde{\theta}}$ term, while normal load fluctuations are primarily driven by the $\tilde{\alpha}$ term. Figure 6d and Fig. 6e show the makeup and phase relationships of the tyre longitudinal force. The contribution from the tyre slip $\tilde{F}_{\text{x}}(\sigma_{\text{x}})$ is 180° out of phase with the slip velocity $\tilde{V}_{\text{sx}}$ which makes it dissipative, while the phase for the normal load term is 32.1° and is the main contributor to instability (all other terms from Eqn. (12) are negligible). This shows that the tyre force gradient terms $C_{\sigma_x,x}$ and $C_{F_z,x}$ have major influences on stability, which is further supported in the following sections.

3.4 Eigenvalue Sensitivity

To investigate the stability boundary of the driveline mode, eigenvalue sensitivity is calculated using the eigenvalue perturbation method [27]. This gives the gradient of the eigenvalue of interest with respect to changes in model parameters, allowing the stability boundary sensitivity to be discerned. The sensitivity of an eigenvalue λ_{i} with respect to a parameter τ, on which the system matrix $\mathbf{A}$ depends, is defined as:

$$\frac{\partial \lambda_{\text{i}}}{\partial \tau} = \mathrm{y}_{\text{i}}^{\text{T}} \frac{\partial \mathbf{A}(\tau)}{\partial \tau} \mathrm{x}_{\text{i}} \tag{25}$$

where x_i and y_i are the right and left eigenvectors of λ_{i}, respectively, normalised such that $y_i^T x_i = 1$. The gradient of interest is along the real axis, so the left-hand side of Eqn. (25) is decomposed into:

$$\lambda_{\text{i}}' = \mathrm{Re}\left(\frac{\partial \lambda_{\text{i}}}{\partial \tau}\right) + \mathrm{i}\,\mathrm{Im}\left(\frac{\partial \lambda_{\text{i}}}{\partial \tau}\right) \tag{26}$$

and the real portion is taken as the sensitivity of the stability boundary to parameter τ. These results are then scaled by the magnitude of the parameter ($|\tau|\mathrm{Re}(\lambda_{\text{i}}')$), to make the sensitivities proportional to a fractional change in any parameter.

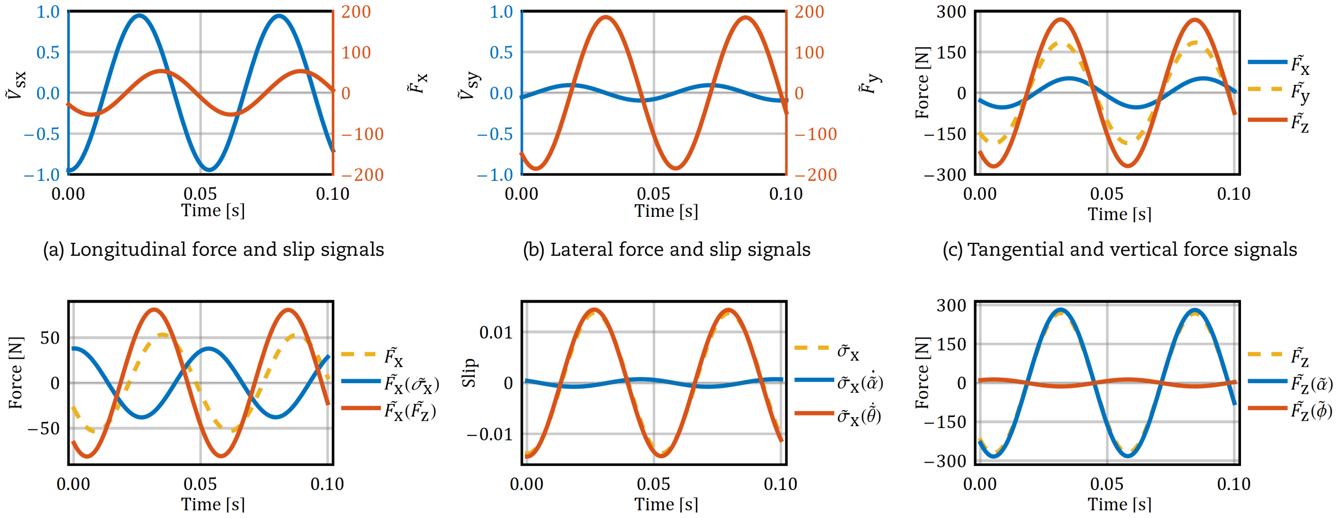

(a) Longitudinal force and slip signals (b) Lateral force and slip signals (c) Tangential and vertical force signals

(d) Makeup of the longitudinal force (e) Makeup of the longitudinal slip (f) Makeup of the vertical load

Fig. 6. Tyre force and slip signals used in the energy analysis.

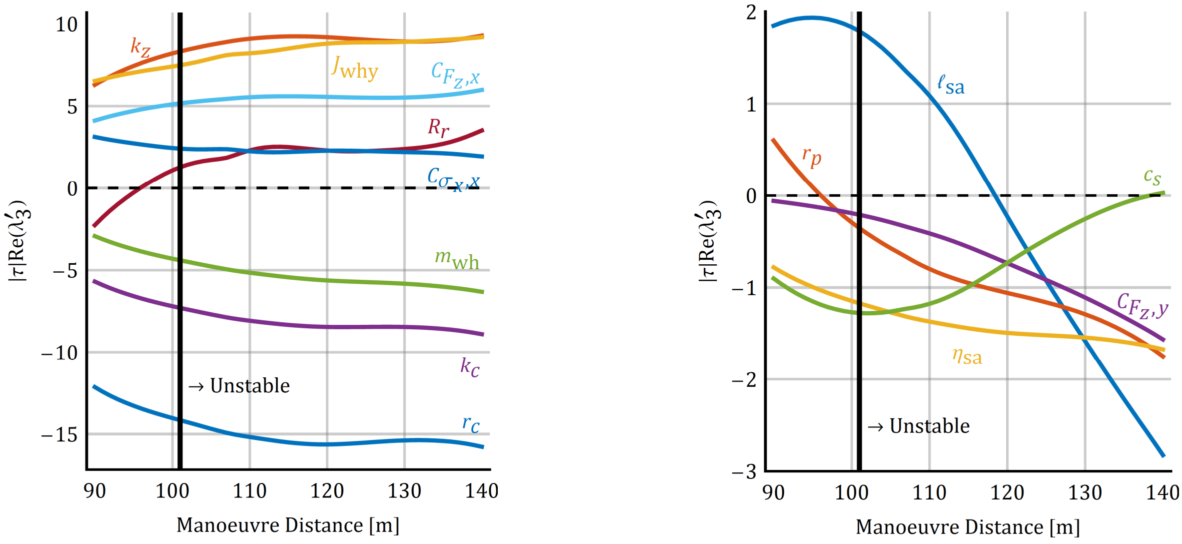

(a) Full Plot (b) Magnified plot

Fig. 7. Sensitivity of the driveline stability boundary with respect to several model reference parameters.

To get a practical understanding of the system's stability boundary, the sensitivity procedure is performed with dimensional model parameters. The parameters to which the stability is most sensitive to, and their evolution during the braking manoeuvre, are presented in Fig. 7. Here the sensitivity of each parameter is shown as they evolve through the quasistatic reference manoeuvre, which reaches instability where the vertical bar is shown on the graphs. A positive sensitivity to a parameter means the system stability decreases with an increase in that parameter, and vice versa. The parameters with the biggest effect can be grouped into:

1) Frequency parameters: those that effect the natural frequencies of the driveline and rear hop modes, such as tyre vertical stiffness k_z, chain stiffness k_c, rear sprocket ratio r_c (which is prominent in the equivalent chain stiffness about the wheel axis), wheel moment of inertia J_{why}, wheel mass m_{wh}, and swingarm mass position η_{sa};
2) Tyre force gradient parameters: $C_{\sigma_x,x}$, $C_{F_z,x}$, and $C_{F_z,y}$; and,
3) Geometric parameters: those that effect chain geometry and the chain matrix, such as front sprocket radius r_p, and tyre outer radius R_r.

As expected, system damping c_s produces a small stabilising effect. Swingarm length l_{sa} has a significant yet complicated effect, as it crosses the x-axis meaning the sensitivity changes sign and any stabilising effects will be reversed after that point. This is assumed to be due to its appearance throughout many of the system's terms.

To test the results of the sensitivity analysis presented in Fig. 7, the stability regions of the nondimensional equations of motion (16) are plotted with varying parameter inputs. These regions are calculated using the Routh-Hurwitz criterion of the system's characteristic polynomial and are shown in Fig. 8. The regions are plotted with respect to the nondimensional tyre force gradient parameters to facilitate comparisons to previous studies [12], and each subfigure has a nondimensional parameter selected from the groups above varied by ±10%. The top row shows that varying the frequency parameters $\mathcal{J}_\theta$ and Φ_c have a large effect on the stability boundary, as does the manoeuvre-dependent slip parameter ν_x. The second row confirms that geometric parameters ξ_R and σ have a smaller effect, similar to that of the system damping ζ. There is agreement both between the eigenvalue sensitivities and their respective changes in stability regions, and with previous work [12], where $\lambda_{x1} \cong \lambda$ and $\gamma_{xx} \cong -\gamma$ and Fig. 8 can be compared to the general case presented there.

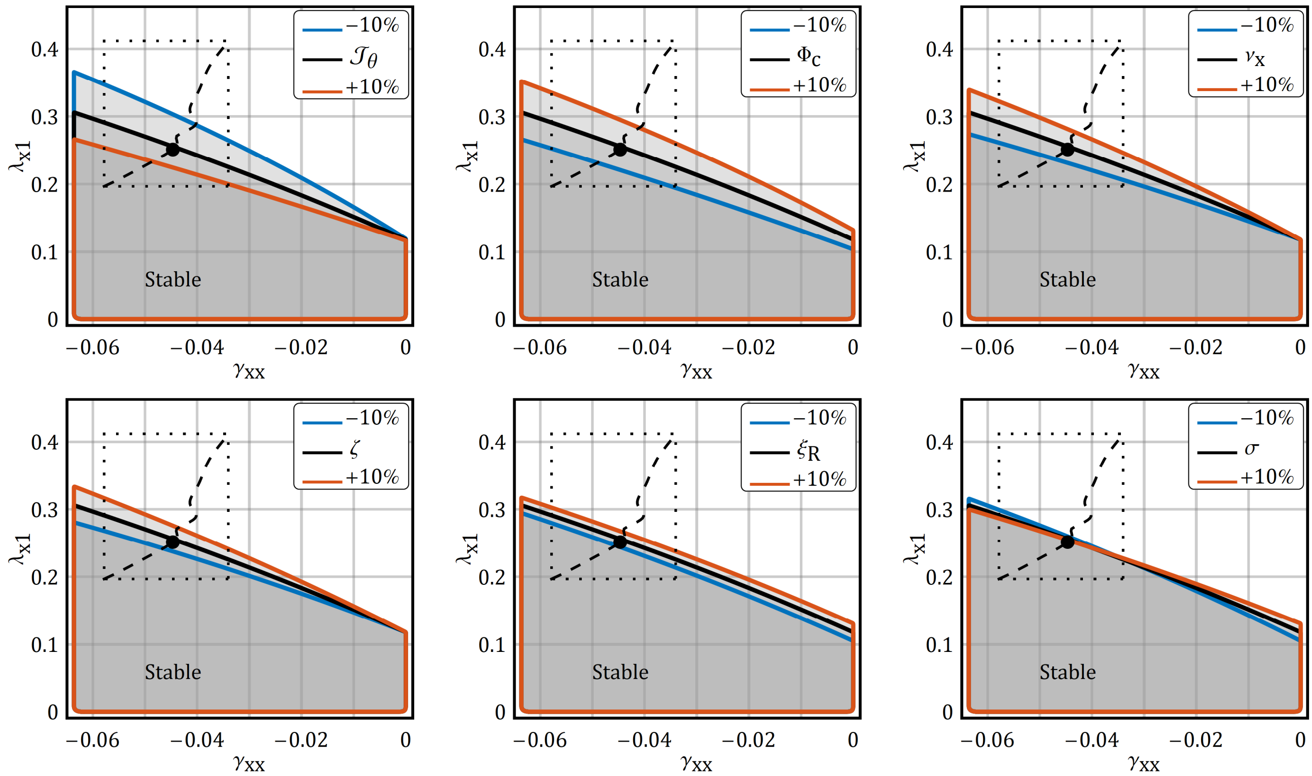

Fig. 8. Stability regions with respect to non-dimensional parameters. The black point gives the linearisation point, the dotted box shows the region boundaries, and the dashed line traces the whole manoeuvre.

Finally, an attempt is made to determine the symbolic underpinnings of the eigenvalue sensitivities found in Fig. 7, by investigating the complete linearised equations of motion (16). The main matrices (mass, damping, and stiffness) are all positive semidefinite, and the asymmetric factor ξ_R in the chain matrix remains close to one, making it effectively symmetric. This leaves the system stability to depend mainly on the tyre slip matrices, as supported by the above findings. Negative terms in the diagonal of the damping matrix lead to decreased stability, as do asymmetric terms in both the damping and stiffness matrices [28]. Reducing the total damping and total stiffness matrices by removing negligible and unimportant terms gives:

$$\hat{\mathbf{C}} = \mathbf{C} + \mathbf{C}_{\text{tyre}} = 2\zeta\nu_x\omega_n \begin{bmatrix} \cdots & \nu_x(\tau_\alpha\gamma_{xx} - s_\phi\gamma_{yx}) & \cdots \\ \tau_\alpha\gamma_{xx} - s_\phi\gamma_{xy} & -\nu_x\gamma_{xx} & \cdots \\ \cdots & \cdots & \cdots \end{bmatrix} \tag{27}$$

$$\hat{\mathbf{K}} = \mathbf{K} + \mathbf{K}_{\text{chain}} + \mathbf{K}_{\text{tyre}} = \omega_n^2 \begin{bmatrix} \cdots & \delta\sigma\Phi_c & \cdots \\ \delta\xi_R\sigma\Phi_c - \lambda_{x1} & \Phi_c & \cdots \\ \cdots & \cdots & \cdots \end{bmatrix} \tag{28}$$

where the role some of the important parameters can be seen. The factors ζ and ν_x tend to increase damping in scalar manner. The tyre slip term γ_{xx}, normally negative in regular operation of the tyre, gives positive damping to the matrix. If this term changes sign, such as when peak tyre grip is exceeded, it introduces negative damping to the diagonal term which can lead to instability. The tyre slip terms γ_{xy}, γ_{yx} and λ_{x1} influence the asymmetry of both matrices, and show increased stability when reduced. In the case of γ_{yx}, the asymmetry is multiplied by ν_x, but the scalar damping effect of ν_x is stronger than its asymmetric effect. The parameter ξ_R also brings about asymmetry in the total stiffness matrix (28), but its value tends to stay close to unity, affected by tyre toroidal geometry and rolling radius characteristics. Finally, the chain geometry term σ links the α and θ equations in the total stiffness matrix (28), where asymmetry introduced by λ_{x1} can cause instability.

3.5 Stabilisation via Natural Frequencies

Figure 9 shows the changes in the eigenvalues with respect to the parameters that effect the natural frequencies of the driveline and rear hop modes. It can be seen on the right of the figure that with stabilising changes in k_c, r_c, or J_{why}, the driveline mode's natural frequency is raised and damping increased. While on the left of the figure, with stabilising changes to k_z or m_{wh}, the rear hop mode's frequency is lowered, and damping of the driveline mode is increased. This result suggests that a separation of the natural frequencies of the two modes leads to more stable behaviour.

3.6 Stabilisation via Chain Geometry

Another stabilising factor found is the chain geometry factor σ, although this parameter is highly based on the manoeuvre and dependent on swingarm angle α. The stability with respect to varying σ is shown in Fig. 10a. An interesting insight is that there can be a stabilising effect by *increasing* σ (and therefore increasing the chain-to-swingarm angle ψ), but that effect quickly vanishes as the system approaches instability. A parallel swingarm and chain ($\sigma = 0$) remains stable throughout the whole manoeuvre. The change in sign of the eigenvalue sensitivity is due to the gradient of these curves.

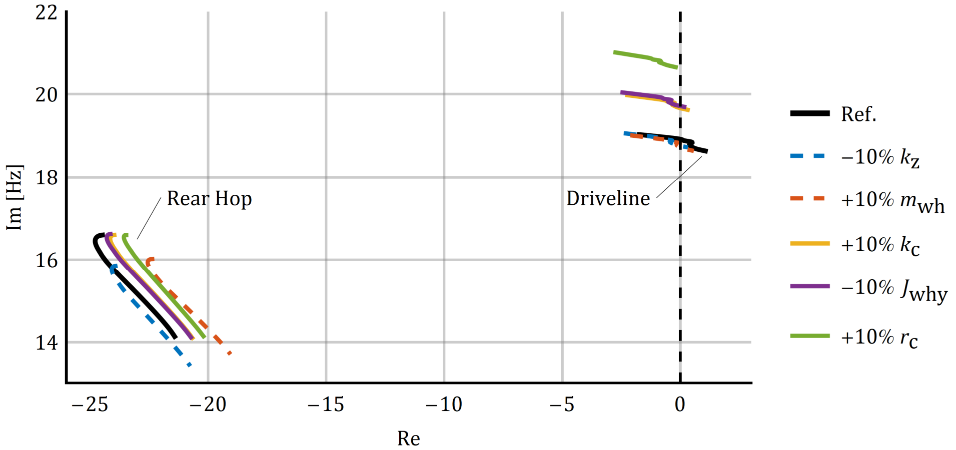

Fig. 9. Changes to eigenvalues with respect to natural frequency parameters.

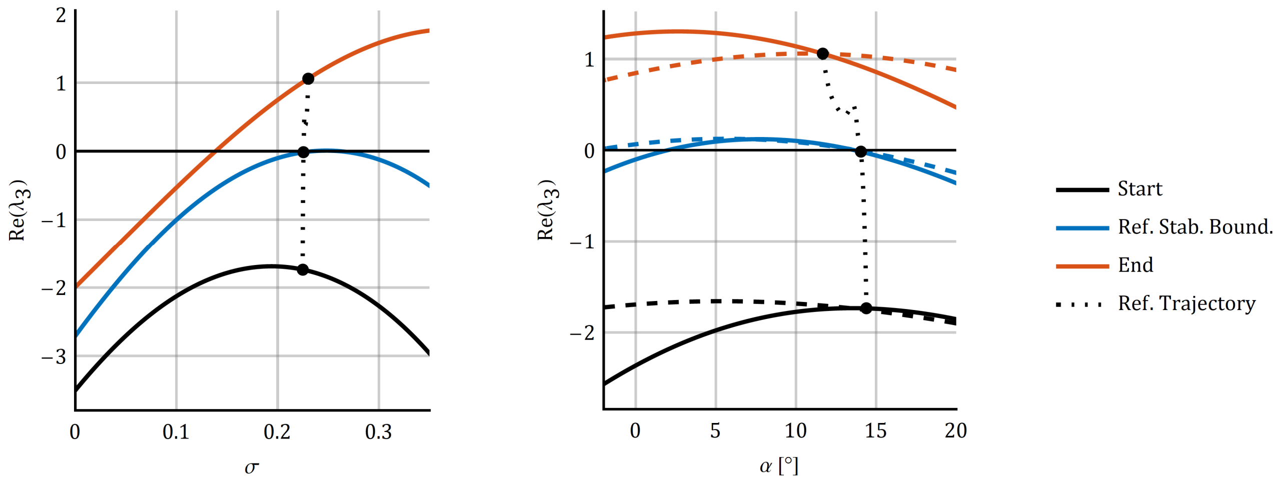

(a) Chain geometry σ

(b) Swingarm angle α

Fig. 10. Stability with varying chain geometry σ and swingarm angle α. Solid lines represent the region's beginning, end, and reference stability boundary, while the dashed lines represent the same analysis with a frozen chain geometry (σ = 0.23). The black dotted line shows the manoeuvre's reference trajectory.

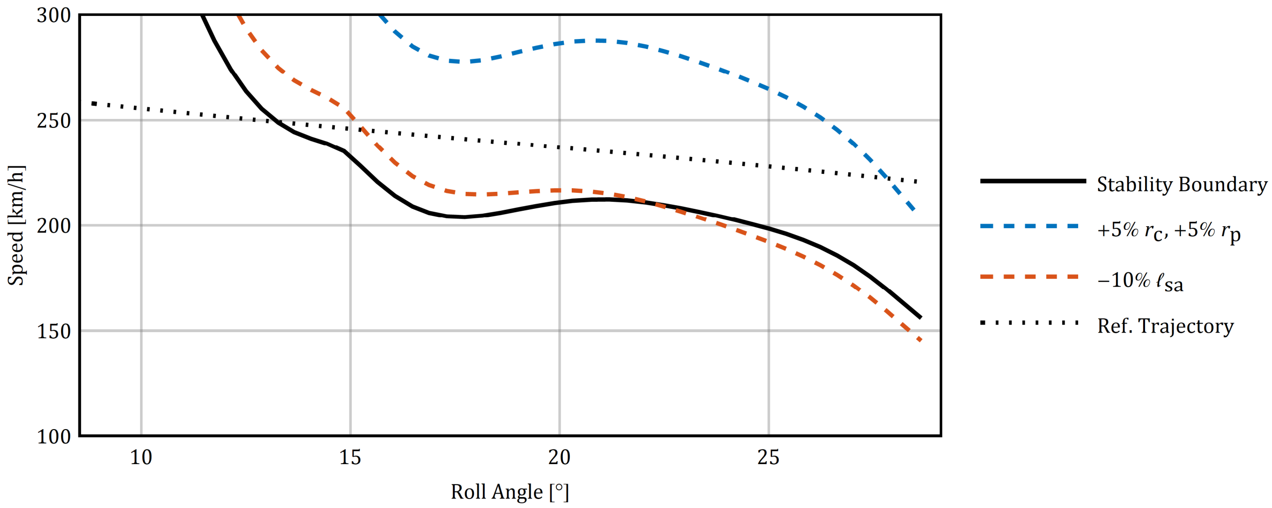

Fig. 11. Driveline stability boundary with respect to forward speed V_{fx} and roll angle ϕ, along with some altered parameter boundaries to show stabilising effects.

3.7 Effect of Swingarm Angle Equilibrium Condition

The effects of swingarm length are fairly complex, as it is a characteristic length of the system and appears throughout the equations of motion. It also is not an effective parameter for stabilising the system, due to its sensitivity gradient changing sign as seen in Fig. 7. In contrast, the swingarm equilibrium angle, which can effectively be set by the parameter h_f, does have a significant effect since it changes the chain geometry, which has an effect on stability as the last section shows. To discern between the effects of chain geometry and a possible secondary effect of swingarm angle, analysis is performed with a chain geometry factor σ frozen at a value of 0.23, see Fig. 10b.

While the non-frozen analysis shows a negative gradient as swingarm angle is increased (moving towards a parallel swingarm and chain), the frozen analysis loses this effect, and the dashed curves show flatter behaviour. There is a small secondary effect, with the manoeuvre operating close to the peak of instability on the α -curves. In the stable region, an increase in swingarm angle leads to higher stability (with frozen chain geometry), while in the unstable region the effect is reversed with a more horizontal swingarm being more stable. Note that the main effect of braking moment M_{brake} is the change in the stationary swingarm value α_0, and thus σ, and therefore would affect system stability. Unfortunately, this cannot be properly captured in the linearized minimal model analysis.

3.8 Effect of Roll Angle Equilibrium Condition

The effect of roll angle on stability is difficult to characterise with the simplified model due to so many externally determined equilibrium value dependencies. For example: the vertical height of point F, z_f, depends on ϕ, as do many of the tyre parameters. To view the effects of roll angle on system stability, the stability boundary with respect to the forward speed V_{fx} (critical speed) is determined during the manoeuvre as roll angle increases. This is shown in Fig. 11, along with similar manoeuvres with altered parameters to display some of the stabilising and destabilising effects they can have. The increase in rear sprocket radius (with corresponding increase in front sprocket radius to maintain final drive ratio) proves to be a useful adjustment in stabilising the system as described previously. The shortening of the swingarm length also initially shows increased stability, but at 21° of roll angle the effect is reversed. The conclusion from this figure is that with increased roll angle, the stability of the system with respect to forward speed decreases.

The decrease in system stability is not directly due to the presence of roll angle in the dynamics, seen in the eigenvector plot in Fig. 5d, but due to some indirect effect on other equilibrium parameters. As shown in Fig. 7, the tyre force gradient parameters $C_{\sigma_x,x}$ and $C_{F_z,x}$ have a large effect on stability and are also highly dependent on roll angle (tyre camber). This effect is highlighted in Fig. 12 where an increase in roll angle shows destabilising changes in tyre force gradient parameters, as proven in the energy and sensitivity analyses. This is the method by which increasing the roll angle ϕ indirectly destabilises the system. Further investigations into the effect of roll angle on system stability would require a more complete multibody model, but the current results suggest that the two degree of freedom model presented in [12] could be augmented to include a quasistatic roll angle parameter for increased accuracy during braking manoeuvres that include a leaning motorcycle.

3.9 Remarks on Relaxation Length and Nonlinear Effects

In the adopted model the effects of tyre relaxation have been considered negligible, as in other similar studies [12, 13]. It should be recalled, however, that increasing the relaxation length to sufficiently high values would produce destabilizing effects on the model, reducing the interval of stability with respect to travelling speed [9]. An effect that can be explained considering that tyre relaxation influences the phase-lag between the factors of the power exchanged at the ground contact point (and thus the energy flow), which is able to bring the system to critical conditions.

As a final remark, for assessing the validity of the presented linear analysis in predicting stability, the post-bifurcation behaviour of the related nonlinear system should be investigated, focusing on bifurcation diagrams and existence of limit cycles. Some preliminary results on the effects of nonlinear terms on this kind of self-excited oscillation have recently been presented in [29], showing that the nonlinear system (at zero roll angle) has a non-critical behaviour, with a single stable limit cycle in the parameter domain of technological interest, and growing with linearised instability, suggesting that the linearised model is valid in predicting stability.

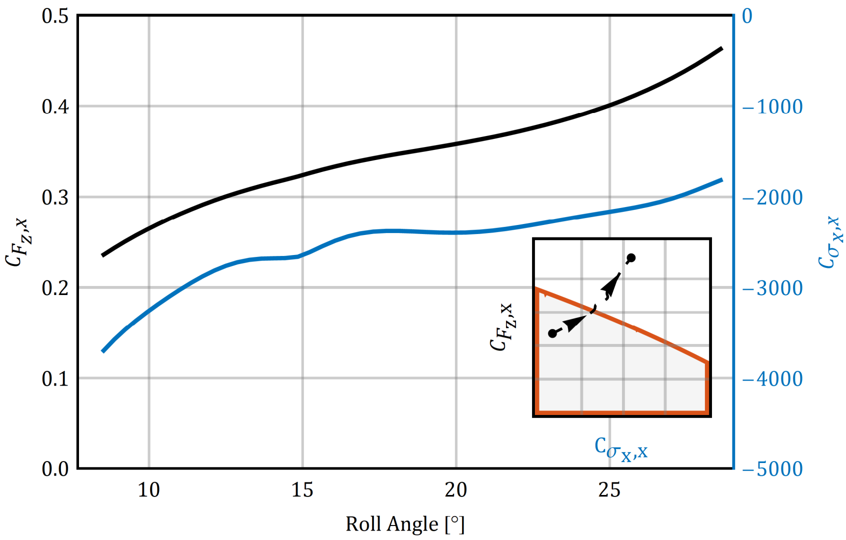

Fig. 12. Tyre tangential force gradient parameters as a function of roll angle. Inset is the tyre gradient domain showing the stable region and the manoeuvre proceeding to unstable.

4. Conclusions

In this study a new simplified model of the rear of a motorcycle was developed with a three degrees of freedom framework that includes the lateral dynamics introduced by roll angle. This allows the expansion of previous works from straight braking investigation into more complex manoeuvres. The model is linearised about equilibrium values in a quasistatic braking region and linear methods such as eigensystem analysis, eigenvalue sensitivity, and Routh-Hurwitz stability criterion are used, as well as an energy flow analysis to detect sources of instability.

Results agree with those in [12], showing an unstable driveline mode with a frequency of around 19 Hz. Instability arises from the longitudinal force affected by tyre force gradient parameters $C_{\sigma_x,x}$ and $C_{F_z,x}$ and the phase relationship between swingarm angle $\tilde{\alpha}$ and wheel speed $\dot{\tilde{\theta}}$ oscillations. It is found that the biggest factor to stability is the natural frequencies of the driveline and rear hop modes, parameters such as tyre vertical stiffness k_z, chain stiffness k_c, rear wheel mass m_{wh}, rear wheel inertia J_{why}, and rear sprocket radius r_c having the greatest effect. Stabilisation can also be achieved by reducing the chain-to-swingarm angle ψ, while the effect of the equilibrium value of swingarm angle is minimal when ψ is held constant. The out-of-plane dynamics did not play a role in the stability of the system, as supported by the eigenvectors and the energy flow analysis, but the equilibrium value of the roll angle plays a significant role through its effect on the tyre force gradient parameters $C_{\sigma_x,x}$ and $C_{F_z,x}$, both of which move in a destabilising direction as roll angle is increased.

Future work will include investigating mid-corner and acceleration manoeuvres at high roll angle, using the minimal model to analyse the stability of the rear swingarm system. The model will also need to be validated in these conditions, again using a complex multibody simulation. These operating conditions, and the stability of the rear swingarm system within them, are not yet studied in literature. The results here only explore a part of the potential of the developed model. Further, an augmentation could be made to the minimal model parameters so as to simulate a torsional degree of freedom in the swingarm pivot and be used to investigate the swingarm's torsional rigidity and its effects on stability.

Author Contributions

A.E. Schramm contributed by developing the model and the calculations; L. Leonelli contributed by providing experimental data and analysing the results; S. Sorrentino contributed with the planning and with analysing the results. The manuscript was written through the contribution of all authors. All authors discussed the results, reviewed, and approved the final version of the manuscript.

Acknowledgments

The authors have no acknowledgments to make for the present work.

Conflict of Interest

The authors declared no potential conflicts of interest with respect to the research, authorship, and publication of this article.

Funding

The authors received no financial support for the research, authorship, and publication of this article.

Data Availability Statement

All data generated or analysed during this study are available from the corresponding author upon reasonable request.

Nomenclature

α	Swingarm angle
α_{s0}	Suspension spring preload
α_{slip}	Slip angle
β_p	Front sprocket locating angle
χ_i	Compact notation for tyre force gradient terms
δ	Chain activation (1 for braking and –1 for acceleration)
ϕ	Roll angle
ϕ_{f0}	Frame torsional spring preload
Γ_i	Linear combination of the γ_{ij} coefficients
γ_{ij}	Damping terms arising from ground tyre forces
Φ_i	Normalised stiffness coefficients
η_{fr}	Locating variable for frame centre of mass
η_{sa}	Locating variable for swingarm centre of mass
φ	Spin slip
λ_{ij}	Compact notation for tyre force gradient terms
ν_i	Normalised velocity component
θ	Wheel angular displacement
ρ_r	Toroid radius of the tyre
I_i	Normalized inertia coefficient
$\mathbf{J}_{fr}$	Inertia matrix of the rolling frame
$\mathbf{J}_{sa}$	Inertia matrix of the swingarm
$\mathbf{J}_{wh}$	Inertia matrix of the rear wheel
J_α	Reduced moment of inertia about α
J_ϕ	Reduced moment of inertia about ϕ
$\mathbf{K}$	Stiffness matrix
k	Total stiffness of the system
k_f	Torsional stiffness at the frame joint F
k_s	Torsional stiffness at the swingarm pivot S
L_R	Characteristic length
l_α	Characteristic length
l_ϕ	Characteristic length
l_c	Dynamic total length of the chain
l_p	Front sprocket locating distance
l_{tc}	Tangential length of the taut branch of the chain
Δl_c	Equilibrium chain stretch
l_{fc}	Free total length of the chain

σ, σ'	Chain geometry characteristic coefficients	$\mathbf{M}$	Mass matrix
τ_x	Compact notation for tan(x)	M_{brake}	Braking moment
Ω_f	Angular speed of the frame (stationary)	$M_{cent,i}$	Centrifugal moment
ω	Angular speed of wheel	$M_{cor,i}$	Coriolis moment
ω_n	Natural frequency resulting from normalisation	$M_{gyro,i}$	Gyroscopic moment
ξ_i	Near-unit dimensionless geometric factor	m_{fr}	Mass of the rolling frame
ψ	Chain angle	m_{sa}	Mass of the swingarm
ψ_f	Normalised rotational damping coefficient	m_{wh}	Mass of rear wheel
ζ	Normalised Damping ratio	$\mathbf{q}$	Vector of Lagrangian coordinates
$\mathbf{C}$	Damping matrix	R_c	Loaded radius
$C_{i,j}$	Components of the tyre force gradients	R_R	Rolling radius
c_f	Torsional damping coefficient at the frame joint F	R_r	Outer radius of the wheel
c_s	Torsional damping coeff. at the swingarm pivot S	r_c	Radius of rear sprocket
c_x	Compact notation for cos(x)	r_p	Radius of front sprocket
d	Sprocket centre distance	s_x	Compact notation for sin(x)
ΔE_i	Energy variation over a period T	T	Period of oscillation
F_c	Chain elastic force	V_f	Velocity of the frame (stationary)
F_R	Planar resultant of combined forces F_x, F_y	V_{sx}, V_{sy}	Slip velocity components
F_x, F_y, F_z	Tyre ground force components	x, y, z	Coordinates of reference system
g	Acceleration due to gravity	x_f	In-plane distance from point S to point F in x direction
h_f	Distance from point S to point F normal to x direction	z_f	Height of point F from ground plane

Appendix

Tyre Notation

$$\nu_x = \frac{V_{fx}}{R_{R0}\omega_0}, \quad \nu_y = \frac{V_{fy}}{R_{R0}\omega_0}, \quad \nu_\psi = \frac{\Omega_{fz}}{R_{R0}\omega_0} \tag{A1}$$

$$\chi_x = C_{\sigma_x,x}\nu_x + C_{\sigma_y,x}\nu_y + \left[C_{\sigma_x,x}\sin(\phi_0)L_R - C_{\sigma_y,x}(x_f + l_{sa}\cos(\alpha_0))\right]\nu_\psi \tag{A2}$$

$$\chi_y = C_{\sigma_x,y}\nu_x + C_{\sigma_y,y}\nu_y + \left[C_{\sigma_x,y}\sin(\phi_0)L_R - C_{\sigma_y,y}(x_f + l_{sa}\cos(\alpha_0))\right]\nu_\psi \tag{A3}$$

$$\lambda_{x1} = c_\phi C_{F_z,x}\Phi_z - c_\phi^2 \frac{\eta}{kR_{R0}}\chi_x - \frac{1}{k}\left(s_\phi C_{\sigma_x,x} + \tau_\alpha C_{\sigma_y,x}\right)\nu_\psi \tag{A4}$$

$$\lambda_{x2} = \tau_\phi C_{F_z,x}\Phi_z + \frac{1}{k}\left[\frac{1}{l_\phi}\left(C_{\phi,x} - \tau_\phi \frac{\eta R'^{\phi}_{c0}}{R_{R0}}\chi_x\right) + C_{\sigma_x,x}\nu_\psi\right] \tag{A5}$$

$$\lambda_{y1} = c_\phi C_{F_z,y}\Phi_z - c_\phi^2 \frac{\eta}{kR_{R0}}\chi_y - \frac{1}{k}\left(s_\phi C_{\sigma_x,y} + \tau_\alpha C_{\sigma_y,y}\right)\nu_\psi \tag{A6}$$

$$\lambda_{y2} = \tau_\phi C_{F_z,y}\Phi_z + \frac{1}{k}\left[\frac{1}{l_\phi}\left(C_{\phi,y} - \tau_\phi \frac{\eta R'^{\phi}_{c0}}{R_{R0}}\chi_y\right) + C_{\sigma_x,y}\nu_\psi\right] \tag{A7}$$

$\mathbf{K}_{chain}$ Matrix

$$\sigma = \frac{\sin(\psi_0)R_{c0}}{c_\alpha r_c}, \quad \sigma' = \left(\frac{1}{l_{tc0}} - \frac{1}{l_{sa}\cos(\psi_0)}\right)\frac{\Delta l_c}{\tan^2(\psi_0)} \tag{A8}$$

$\mathbf{C}_{tyre}$ Matrix

$$\gamma_{xx} = \frac{C_{\sigma_x,x}l_\alpha^2}{c_s V_{fx}}, \quad \gamma_{xy} = \frac{C_{\sigma_y,x}l_\alpha^2}{c_s V_{fx}}, \quad \gamma_{yx} = \frac{C_{\sigma_x,y}l_\alpha^2}{c_s V_{fx}}, \quad \gamma_{yy} = \frac{C_{\sigma_y,y}l_\alpha^2}{c_s V_{fx}} \tag{A9}$$

$$\Gamma_x = \gamma_{xx}\nu_x + \gamma_{xy}\nu_y + \left[\gamma_{xx}\tau_\phi l_\phi - \gamma_{xy}(x_f + l_\alpha)\right]\nu_\psi \tag{A10}$$

$$\Gamma_y = \gamma_{yx}\nu_x + \gamma_{yy}\nu_y + \left[\gamma_{yx}\tau_\phi l_\phi - \gamma_{yy}(x_f + l_\alpha)\right]\nu_\psi \tag{A11}$$

Equations of Motion Notation

$$\omega_n = \sqrt{\frac{k}{m_\alpha}}, \quad \zeta = \frac{c_s}{2l_\alpha^2\sqrt{km_\alpha}} \tag{A12}$$

$$J_\alpha = J_{say} + l_{sa}^2(m_{sa}\eta_{sa}^2 + m_{wh}) \tag{A13}$$

$$J_\phi = J_{frx} + J_{whxz} + J_{sax}\cos^2(\alpha) + J_{saz}\sin^2(\alpha) \tag{A14}$$

$$m_\alpha = \frac{J_\alpha}{l_\alpha^2}, \quad I_\theta = \frac{J_{why}}{m_\alpha R_{c0}R_{R0}}, \quad I_\phi = \frac{J_\phi}{m_\alpha l_\phi^2} \tag{A15}$$

$$\psi_f = \frac{c_f l_\alpha^2}{c_s l_\phi^2}, \quad \Phi_c = \frac{k_c r_c^2}{kR_{c0}R_{R0}}, \quad \Phi_z = \frac{k_z}{k}, \quad \Phi_f = \frac{k_f}{kl_\phi^2}, \tag{A16}$$

$$k = \frac{k_s}{l_\alpha^2} + k_z\cos^2(\phi_0) + \frac{\tau_\alpha c_\phi(\eta_{sa}m_{sa} + m_{wh})}{l_\alpha}g \tag{A17}$$

$$g_{\alpha\phi} = \frac{\eta_{sa}m_{sa} + m_{wh}}{kl_\phi}g \tag{A18}$$

$$g_\phi = \frac{c_\phi\left[(\eta_{fr}m_{fr} + m_{sa} + m_{wh})h_f + \tau_\alpha(\eta_{sa}m_{sa} + m_{wh})l_\alpha\right]}{kl_\phi^2}g \tag{A19}$$

$$\xi_z = \frac{z_f}{l_\phi}, \quad \xi_R = \frac{R_{c0}}{R_{R0}} \tag{A20}$$

References

[1] Manrique-Escobar, C.A., Pappalardo, C.M, Guida, D., On the Analytical and Computational Methodologies for Modelling Two-wheeled Vehicles within the Multibody Dynamics Framework: A Systematic Literature Review, *Journal of Applied and Computational Mechanics,* 8(1), 2022, 153-181.
[2] Martini, A., Bellani, G., Fragassa, C., Numerical Assessment of a New Hydro-Pneumatic Suspension System for Motorcycles, *International Journal of Automotive and Mechanical Engineering,* 15(2), 2018, 5308-5325.
[3] Tezuka, Y., Kokubu, S., Shiomi, Y., Kiyota, S., Vibration Characteristics Analysis in Vehicle Body Vertical Plane of Motorcycle during Turning, *Honda R&D Technical Review,* 16(1), 2004, 219-224.
[4] Catania, G., Mancinelli, N., Motorcycle Local Stability Analysis Under Acceleration and Braking by Model Linearization and Eigenproblem Solution, *ASME International Design Engineering Technical Conferences and Computers and Information in Engineering Conference (IDETC 2007)*, Las Vegas, NV, USA, 2007.
[5] Catania, G., Mancinelli, N., Modeling Nonlinear Motorcycle Dynamical Behavior During Severe Acceleration and Braking, *ASME International Mechanical Engineering Congress and Exposition (IMECE 2008)*, Boston, MA, USA, 2008.
[6] Cossalter, V., Lot, R., Massaro, M., The chatter of racing motorcycles, *Vehicle System Dynamics,* 46(4), 2008, 339-353.
[7] Cossalter, V., Lot, R., Massaro, M., The Significance of Powertrain Characteristics on the Chatter of Racing Motorcycles, *ASME Engineering Systems Design and Analysis (ESDA 2012)*, Nantes, France, 2012.
[8] Sharp, R.S., Watanabe, Y., Chatter vibrations of high-performance motorcycles, *Vehicle System Dynamics,* 51(3), 2013, 393-404.
[9] Catania, G., Leonelli, L., Mancinelli, N., A Multibody Motorcycle Model for the Analysis and Prediction of Chatter Vibrations, *ASME International Mechanical Engineering Congress and Exposition (IMECE 2013)*, San Diego, CA, USA, 2013.
[10] Leonelli, L., *Dynamic analysis of the motorcycle chattering behaviour by means of symbolic multibody modelling*, Ph.D. Thesis, Department of Industrial Engineering, University of Bologna, Bologna, Italy, 2014.
[11] Leonelli, L., Mancinelli, N., Sorrentino, S., A Study of Motorcycle Chatter Vibration with Multibody Models of Increasing Complexity, *The Dynamics of Vehicles on Roads and Tracks: Proceedings of the 24th Symposium of the International Association for Vehicle System Dynamics (IAVSD 2015)*, Graz, Austria, 2016.
[12] Sorrentino, S., Leonelli, L., A study on the stability of a motorcycle wheel–swingarm suspension with chain transmission, *Vehicle System Dynamics,* 55(11), 2017, 1707-1730.
[13] Leonelli, L., Cattabriga, S., Sorrentino, S., Driveline instability of racing motorcycles in straight braking manoeuvre, *Proceedings of the Institution of Mechanical Engineers, Part C: Journal of Mechanical Engineering Science,* 232(17), 2018, 3045-3061.
[14] Cattabriga, S., De Felice, A., Sorrentino, S., Patter instability of racing motorcycles in straight braking manoeuvre, *Vehicle System Dynamics,* 59(1), 2021, 33-55.
[15] Romualdi, L., Mancinelli, N., De Felice, A., Sorrentino, S., A new application of the Extended Kalman Filter to the estimation of roll angles of a motorcycle with Inertial Measurement Unit, *FME Transactions,* 48(2), 2020, 255-265.
[16] Pacejka, H.B., *Tire and Vehicle Dynamics*, Butterworth-Heinemann, Oxford, 2012.
[17] Pappalardo, C.M., Lettieri, A., Guida, D., A General Multibody Approach for the Linear and Nonlinear Stability Analysis of Bicycle Systems. Part I: Methods of Constrained Dynamics, *Journal of Applied and Computational Mechanics,* 7(2), 2021, 655-670.
[18] Pappalardo, C.M., Lettieri, A., Guida, D., A General Multibody Approach for the Linear and Nonlinear Stability Analysis of Bicycle Systems. Part II: Application to the Whipple-Carvallo Bicycle Model, *Journal of Applied and Computational Mechanics,* 7(2), 2021, 671-700.
[19] De Rossi, L., Schramm, A., De Felice, A., Multibody Efficiency Analysis of Chain Drives in Racing Motorcycles, *Journal of Applied and Computational Mechanics,* 8(3), 2022, 1091-1102.

[20] Sharp, R.S., Giles, C.G., Motorcycle Front Wheel Patter in Heavy Braking, *Vehicle System Dynamics,* 12(1-3), 1983, pp. 159-160.
[21] Schmeitz, A.J.C., Jansen, S.T.H., Tezuka, Y., Hasegawa, M., Miyagishi, S., Application of the Rigid Ring Model for Simulating the Dynamics of Motorcycle Tyres on Uneven Roads, *Bicycle and Motorcycle Dynamics 2010 Symposium on the Dynamics and Control of Single Track Vehicles*, Delft, The Netherlands, 2010.
[22] Guiggiani, M., *The Science of Vehicle Dynamics: Handling, Braking, and Ride of Road and Race Cars*, Springer, Cham, 2018.
[23] Rosenbrook, H.H., The stability of linear time-dependent control systems, *International Journal of Electronics,* 15(1), 1963, 73-80.
[24] Salisbury, I.G., Limebeer, D.J.N., Tremlett, A., Massaro, M., The unification of acceleration envelope and driveability concepts, *The Dynamics of Vehicles on Roads and Tracks: Proceedings of the 24th Symposium of the International Association for Vehicle System Dynamics (IAVSD 2015)*, Graz, Austria, 2016.
[25] Leonelli, L., Limebeer, D.J.N., Optimal control of a road racing motorcycle on a three-dimensional closed track, *Vehicle System Dynamics,* 58(8), 2020, 1285-1309.
[26] Kröger, M., Neubauer, M., Popp, K., Experimental Investigation on the Avoidance of Self-Excited Vibrations, *Philosophical Transactions of the Royal Society A: Mathematical, Physical and Engineering Sciences,* 366(1866), 2008, 785-810.
[27] Greenbaum, A., Li, R.C., Overton, M.L., First-Order Perturbation Theory for Eigenvalues and Eigenvectors, *SIAM Review,* 62(2), 2020, 463-482.
[28] Hagedorn, P., Eckstein, M., Heffel, E., Wagner, A., Self-Excited Vibrations and Damping in Circulatory Systems, *Journal of Applied Mechanics,* 81(10), 2014, 1-9.
[29] Schramm, A., Sorrentino, S., De Felice, A., Nonlinear investigation into the motorcycle chatter phenomenon using numerical simulation, *2021 JSAE Autumn Congress (Society of Automotive Engineers of Japan)*, online, Japan, 2021.

ORCID iD

Alexander E. Schramm https://orcid.org/0000-0001-6885-9848
Luca Leonelli https://orcid.org/0000-0002-6067-4467
Silvio Sorrentino https://orcid.org/0000-0003-2136-5538

How to cite this article: Schramm A.E., Leonelli L., Sorrentino S. Driveline Stability in Racing Motorcycles: Analysis of a Three Degrees of Freedom Minimal Model, *J. Appl. Comput. Mech.*, 9(2), 2023, 404–418.
https://doi.org/10.22055/jacm.2022.41157.3709